LANGMUIR

pubs.acs.org/Langmuir Article

Soft Wetting: Droplet Receding Contact Angles on Soft Superhydrophobic Surfaces

Youhua Jiang,* Zhijia Xu, Bin Li, Juan Li, and Dongshi Guan

Cite This: *Langmuir* 2023, 39, 15401−15408 Read Online

ACCESS | Metrics & More | Article Recommendations | Supporting Information

ABSTRACT: Despite intensive investigations on the droplet receding contact angle on superhydrophobic surfaces, i.e., a key parameter characterizing surface wettability and adhesion, the quantitative correlation between the surface structure mechanical properties (softness) and the droplet receding contact angles remains vague. By systematically varying the geometric dimensions and mechanical properties of soft pillar arrays, we find that the droplet receding contact angles decrease with the decrease in the pillar spring constant. Most surprisingly, the densely packed pillar arrays may result in larger receding contact angles than those on sparsely packed pillars, opposing the understanding of rigid pillar arrays, where the receding contact angles increase with a decrease in the packing density of pillars. This is attributed to the collective effects of capillarity and elasticity, where the energy consumed by the sliding contact line, the energy stored in the distorted liquid−vapor interface, and the energy stored in the deflected pillar contribute to the droplet depinning characteristics. We develop an analytical model to predict the droplet receding contact angles on soft superhydrophobic pillar arrays with knowledge of the material intrinsic receding contact angle, the pillar geometry, and the pillar mechanical properties. The predictions are corroborated by the experimental data measured in this and prior studies.

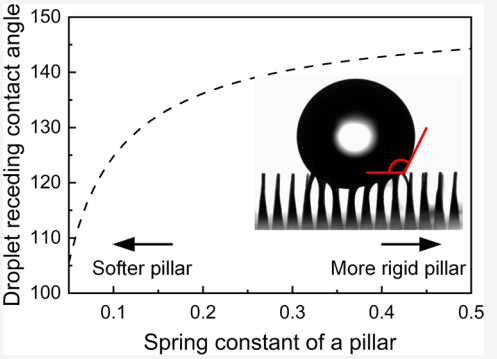

INTRODUCTION

The retention of a fakir (Cassie−Baxter state) droplet to a superhydrophobic surface is critical to various applications, such as thermal management of electronic devices, anti-icing and antibiofouling coatings, and fog collection[1−3]. As a key parameter characterizing droplet retention, the apparent droplet receding contact angle (the droplet contact angle right before the contact line makes an evident retraction) has been intensely studied over the past few decades. Surfaces decorated with hydrophobic pillar arrays are the most studied superhydrophobic surfaces, and a consensus has been reached that the droplet apparent receding contact angle is mainly determined by the material intrinsic receding contact angle θ_r (the apparent receding contact angle measured on the flat surface), the pillar size d, and the pillar center-to-center pitch λ.[4−17]

From the perspective of energy consumption in association with contact line dynamics, the apparent dewetting energy (ΔE_{DW}) required to recede a droplet on rigid superhydrophobic pillar arrays involves the energy consumed by the sliding contact line on pillar tops (ΔE_{CL})[8] and the energy stored in the distorted liquid−vapor interface (ΔE_{LV}),[14,18,19] as

$$\Delta E_{DW} = \Delta E_{CL} + \Delta E_{LV} \quad (1)$$

The energy consumed to laterally dewet a unit area of a flat surface (e_{dw}) is $e_{dw} = \gamma_{SV} - \gamma_{SL} + f_r$, where γ_{SV} is the solid−vapor interfacial tension, γ_{SL} is the solid−liquid interfacial tension, and f_r is a friction force per unit length of contact line, i.e., the force per unit length needed to overcome the contact angle hysteresis in the receding direction.[20−24] Since the force balance along the receding contact line is $\gamma_{LV}\cos\theta_r = \gamma_{SV} - \gamma_{SL} + f_r$, where γ_{LV} is the liquid−vapor interfacial tension, we have $e_{dw} = \gamma_{LV}\cos\theta_r$.

Following Cassie's and Baxter's approach,[25] from the macroscopic perspective, the apparent energy consumed to dewet a unit area of a textured (pillared) surface (e_{DW}) is $e_{DW} = \gamma_{LV}\cos\theta_{R\_R}$, where the subscript R_R denotes the apparent receding contact angle on textured, rigid surfaces. Hence, ΔE_{DW} is $\gamma_{LV}\cos\theta_{R\_R}$ multiplying the apparent boundary length ($2\pi R = n\lambda$, where n is the number of pillars along the droplet boundary and R is the droplet base radius) and the lateral displacement (Δx) of the uniformly receding droplet boundary, as $\Delta E_{DW} = \gamma_{LV}\cos\theta_{R\_R}\cdot n\lambda\Delta x$.

From the microscopic perspective, the energy consumed by the sliding contact line (ΔE_{CL}) is e_{dw} multiplying the area been swept by the microscopic contact line ($\Delta A_{SL\to SV}$) and the energy change in the liquid−vapor interface (ΔE_{LV}) is γ_{LV}, multiplying the change in the liquid−vapor interfacial area

Received: September 8, 2023
Revised: October 9, 2023
Accepted: October 10, 2023
Published: October 19, 2023

(ΔA_{LV}). In the author's prior work,[14] $\Delta A_{SL\to SV}$ is the projected length (L_{CL}) of a contact line that makes a uniform displacement of Δx multiplying n, as $\Delta A_{SL\to SV} = nL_{CL}\Delta x$. The liquid−vapor interfacial area A_{LV} decreases when the contact line slides. This is because the liquid−vapor interface reaches its maximum deformation right before the contact line starts to slide, and hence the sliding of the contact line eases the distortion of the liquid−vapor interface. Here, the decrease in the liquid−vapor interfacial area ΔA_{LV} is considered as a shrinking frontier of the liquid−vapor interface (L_{LV}) that makes lateral displacement (Δx) together with the contact line, as $\Delta A_{LV} = -nL_{LV}\Delta x$.[14] Inserting the expressions of ΔE_{DW}, ΔE_{CL} ($\gamma_{LV}\cos\theta_r \cdot nL_{CL}\Delta x$) and $\Delta E_{LV}(-\gamma_{LV}\cdot nL_{LV}\Delta x)$ into eq 1 and dividing $\gamma_{LV}n\lambda\Delta x$ in both sides, the droplet receding contact angle on a rigid, pillared superhydrophobic surface is

$$\cos\theta_{R\_R} = \cos\theta_r\frac{L_{CL}}{\lambda} - \frac{L_{LV}}{\lambda} = \left(-0.4\frac{d}{\lambda} + 1.4\right)\frac{d}{\lambda}\cos\theta_r - \left(0.5\frac{d}{\lambda} + 1\right)\left(1 - \frac{d}{\lambda}\right) \quad (2)$$

It should be noted that L_{CL} (on a pillar) and L_{LV} (between adjacent pillars) could be approximated as d and $\lambda - d$, respectively.[9,10] Nevertheless, considering the changes in the contact line length and liquid−vapor interface shape when a contact line moves, and most importantly their dependency on the packing density of pillars d/λ,[7] L_{CL}/λ and L_{LV}/λ should be a function of the pillar packing density d/λ and are empirically expressed as $(-0.4d/\lambda + 1.4)\cdot d/\lambda$ and $(0.5d/\lambda + 1)\cdot(1 - d/\lambda)$, respectively[5,14] (please see refs 7 and 14 for more detailed discussion and direct experimental evidence).

Increasing attention has been paid to soft/flexible surfaces such as wearable flexible electronics, underwater soft robotics, and implantable biomedical devices, smart surfaces with flexible structures that respond to external stimuli,[26−29] whose interactions with liquids affect their performance. Since surface softness has been shown to significantly affect the droplet behavior on flat soft surfaces,[30−35] a question arises: will eq 2 developed from rigid surfaces applicable to soft superhydrophobic pillar arrays? This question cannot be answered yet because a quantitative correlation between the droplet apparent receding contact angle and the surface geometrical and mechanical properties remains vague.[36−42] It should be noted that studies investigating completely wetted (Wenzel-state droplets) surface textures are not counted because the object of interest of this study is droplets in the Cassie−Baxter state.[43−45] A clear pillar deflection (Figure 1b) and an evident difference in apparent receding contact angles of evaporating droplets on rigid and soft pillar arrays can be observed (Figure 1c), suggesting that eq 2, which does not consider structure deformation, must not be applicable to soft superhydrophobic surfaces. This highlights the necessity of developing a simple analytical model that predicts the receding contact angles on soft superhydrophobic surfaces.

One of the key bottlenecks of developing analytical models for soft superhydrophobic surfaces is the violation of the small beam deflection assumption (pillar diameter d and pillar tip deflection δ should be much smaller than pillar height h). Pillars produced by conventional photolithography typically have h values smaller than 40 μm, prohibiting a large variation in d while keeping d much smaller than h. Here, using laser drilling, we prepared submillimetric soft pillar arrays with

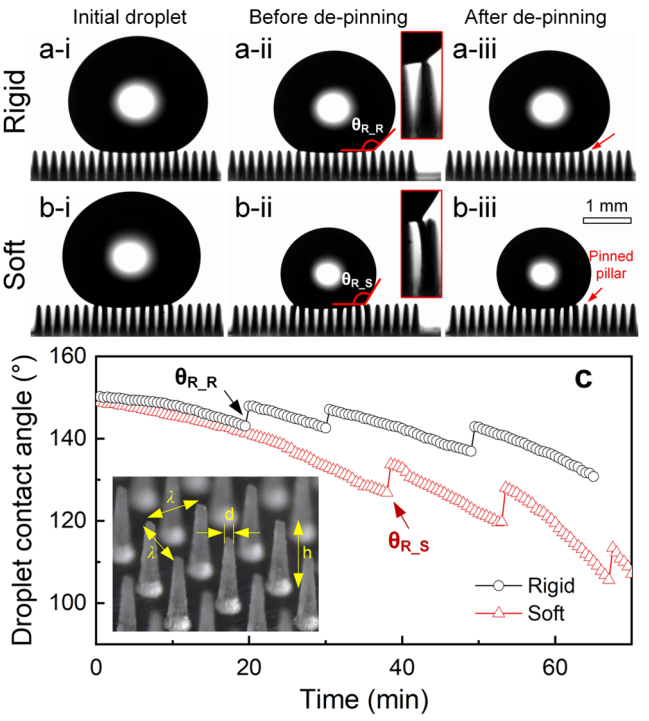

Figure 1. Droplet profiles in evaporation on (a) rigid and (b) soft pillar arrays, whose Young's modulus is 3.5 and 1.0 MPa, respectively. The droplets with initial volumes of 12 μL evaporated at 30 °C and 50% relative humidity and both pillars have heights h of ∼0.55 mm, diameters d of ∼0.045 mm, and pitches λ of 0.2 mm. The droplet shape profiles include (i) the as-deposited droplet, (ii) the last image for the boundary remains pinned on a pillar, and (iii) the first image after the boundary depins (the time interval is 30 s). The inset in (ii) is the amplified image highlighting the pillar shape and deformation. (c) Droplet contact angles in evaporation are plotted with respect to time, where the first receding contact angles on rigid and soft pillar arrays are θ_{R_R} and θ_{R_S}, respectively. The inset is an optical image of pillar arrays with heights of 0.45 mm and a pitch of 0.3 mm.

systematically varying dimensions while not violating the small beam deflection assumption ($d/h < 0.22$ and $\delta/h < 0.29$; see Table S1 in the Supporting Information). This study aims at elaborating the collective effects of capillarity and elasticity on droplet receding contact angles. A simple model that predicts droplet receding contact angles on soft pillar arrays was developed and compared with the experimental data.

MATERIALS AND METHODS

Fabrication of Aluminum Mold. Pores with varying top diameters, bottom diameters, center-to-center pitches, and depths were drilled on polished aluminum plates by using a laser driller (HS50II, Han's Group, China). Because of the nature of laser drilling, that is, the pore diameter decreases as the depth increases, all pores are conical with a top diameter larger than the bottom diameter. The pored aluminum plates were hydrophobilized by 1H, 1H, 2H, 2H-perfluorodecyltrichlorosilane (MACKLIN, China) via chemical vapor deposition.

Fabrication of Pillar Arrays. Soft pillar arrays were replicated from the pored aluminum plates using poly(dimethylsiloxane) (PDMS, Sylgard 184, Dow Corning) solutions with base-to-curing agent ratios of 5:1, 10:1, and 20:1, corresponding to Young's modulus E of around 3.5, 2.6, and 1.0 MPa, respectively. The resulting soft pillar arrays have a top diameter d ranging from 0.02 to 0.10 mm, a base diameter D ranging from 0.09 to 0.18 mm, a center-to-center pitch λ of 0.2 and 0.3 mm, and pillar heights h of around 0.45, 0.55, and 0.65 mm. Pillar geometries and their pillar tip deflections δ were

https://doi.org/10.1021/acs.langmuir.3c02667
Langmuir 2023, 39, 15401−15408

measured optically using ImageJ, as detailed in Table S1. Such pillar geometrical dimensions result in d/λ ranging from 0.07 to 0.53 and the pillar spring constant k ($=3\pi ED^3d/64h^3$) ranging from 0.04 to 2.21 N/m. When the wetting ridge is neglected ($\sim\gamma_{LV}/E$ is in the nanometer scale), the intrinsic receding contact angle θ_r reflects the surface molecular properties and was measured to be 95° on a flat PDMS surface irrespective of the variations in Young's modulus. In addition to the fabrication of submillimetric soft pillar arrays, rigid, cylindrical micropillar arrays, whose structural deformation should be ignored, were also fabricated using PDMS via soft lithography with the base-to-curing agent ratios of 10:1 (see ref 14 for detailed experimental procedures). The pillar height h, diameter d, center-to-center pitch λ, and the corresponding packing density d/λ are 20 μm, 5−50 μm, 10−55 μm, and 0.2−0.91, respectively (see Table S2 for details).

Measurement of Apparent Receding Contact Angles. The droplet apparent receding contact angles were measured using a goniometer (OCA25, Dataphysics, Germany) under room conditions (temperature of 25 °C ± 2 °C, relative humidity of 50% ± 2%, and atmospheric pressure). A deionized water droplet with a volume of 12 μL was produced on the soft pillar arrays by the autodispensing system. The droplet base diameter (>1.8 mm) was much larger than the pillar size so that an axisymmetric circular droplet base was assumed. Then, the needle was attached only to the very top of the droplet, and the liquid was withdrawn at a rate of 0.05 μL/s. Images were taken at a rate of 1 fps, and the contact angles were automatically measured. All reported data are the average of at least 5 reproducible experiments and have error bars of ±2°, which cannot be reflected in the plotted figures.

RESULTS AND DISCUSSION

Experimental Results. Mathematically speaking, eq 2 applies to the entire range of $0 < d/\lambda \leq 1$ because θ_{R_R} equals 180° when $d/\lambda \approx 0$ (a surface with extremely dilute pillars) and θ_{R_R} equals θ_r when $d/\lambda = 1$ (a smooth surface). However, the case with $d/\lambda \approx 0$ cannot be achieved because the liquid impalement (the Cassie-to-Wenzel transition) may occur, whose thresholds depend on the pillar material wettability, height, spacing, and alignment.[46] To validate the model (eq 2) that predicts the receding contact angles for rigid pillar arrays, the measured receding contact angles on micropillar arrays are plotted with respect to the packing density d/λ in Figure 2. An excellent agreement between the measured (orange stars) and predicted values in the range of $0.2 \leq d/\lambda \leq 0.91$ (results shown up to 0.67 in Figure 2) suggests that eq 2 is indeed valid for rigid pillar arrays. However, Figure 2 shows that eq 2 failed to capture the receding contact angles (denoted as θ_{R_S}) on soft pillar arrays, where the subscript R_S represents the apparent receding contact angles on soft surfaces to distinguish itself from the receding contact angles on rigid surfaces R_R. Three interesting findings can be observed: (1) most measured θ_{R_S} are less than those predicted by eq 2, and this deviation increases as d/λ decreases; (2) the most deviated values are the softest pillars with E of 1.0 MPa and heights of 0.65 mm (filled, black circles); (3) eq 2 can still roughly capture θ_{R_S} when d/λ is large (>0.4). The above results reveal the inapplicability of eq 2 to soft superhydrophobic surfaces and confirm that the structural softness indeed affects receding contact angles. As such, we will incorporate the pillar deflection into the droplet-structure interfacial system to develop a new model that predicts droplet receding contact angles on soft pillar arrays.

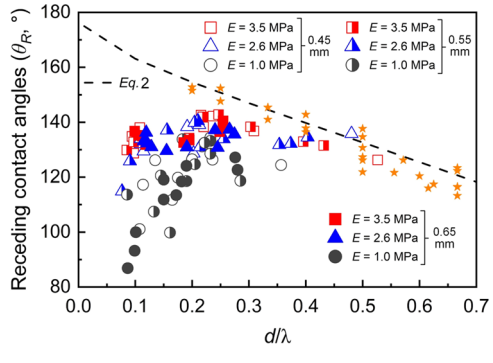

Figure 2. Measured droplet apparent receding contact angles (θ_R) with respect to pillar diameter-to-pitch ratio (d/λ) on pillar arrays with different Young's modulus and pillar heights. The orange stars represent the results on rigid micropillar arrays. The results associated with Young's modulus E of 3.5, 2.6, and 1.0 MPa are represented by red squares, blue triangles, and black circles, respectively. The results associated with pillar heights h of around 0.45, 0.55, and 0.65 mm are differentiated by hollow, hollow-filled, and filled symbols, respectively. The dashed line represents eq 2.

Model Development and Validation. As schematically shown in Figure 3a−3c, for soft superhydrophobic pillar arrays,

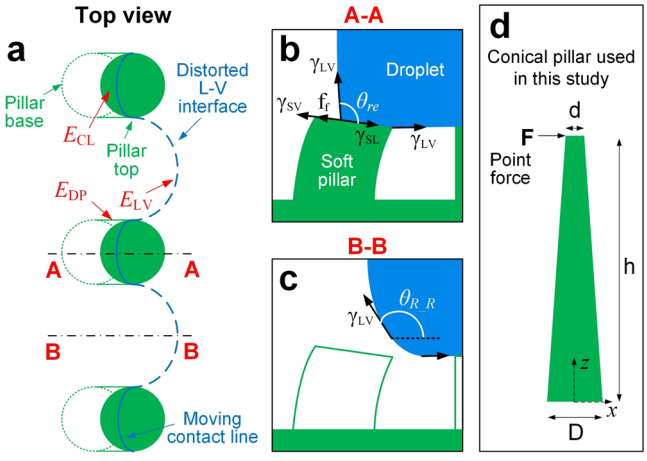

Figure 3. Schematics of the droplet boundary configuration and the associated energies of a receding droplet on soft pillar arrays: (a) top view, (b) side view of the A−A cross section at the pillar tops, and (c) side view of the B−B cross section between two pillars. (d) Geometric dimensions of the conical pillar used in this study.

in addition to ΔE_{CL} and ΔE_{LV}, the energy stored in the deflected soft pillars (ΔE_{DP}) contributes to the apparent energy consumption (or decrease) of the droplet-structure interfacial system ($\Delta E_{DW} = \gamma_{LV}\cos\theta_{R\_S}\cdot n\lambda\Delta x$), as

$$\Delta E_{DW} = \Delta E_{CL} + \Delta E_{LV} + \Delta E_{DP} \quad (3)$$

Here, the wetting ridge along the contact line and its viscoelastic dissipation is not considered as its length scale ($\sim\gamma_{LV}/E$) is only tens of nanometer,[30−33] which is significantly smaller than a conventional poly(dimethylsiloxane) (PDMS) pillar and the droplet. Moreover, small-scale, brittle surface structures (e.g., silicon nanorods) could be damaged by γ_{LV},[47] causing permanent surface deterioration. However, it is not considered for submillimetric, elastomer pillars used in this study.

The pillar can be considered as a vertically placed conical cantilever beam with a linearly varying diameter from D at the base ($z = 0$) to d at the top ($z = h$) and is subject to a horizontal point force (F) at its top (Figure 3d). Hence, the pillar has a moment of inertia of $I(z) = \pi d(z)^2/64$ and $d(z) =$

https://doi.org/10.1021/acs.langmuir.3c02667
Langmuir 2023, 39, 15401−15408

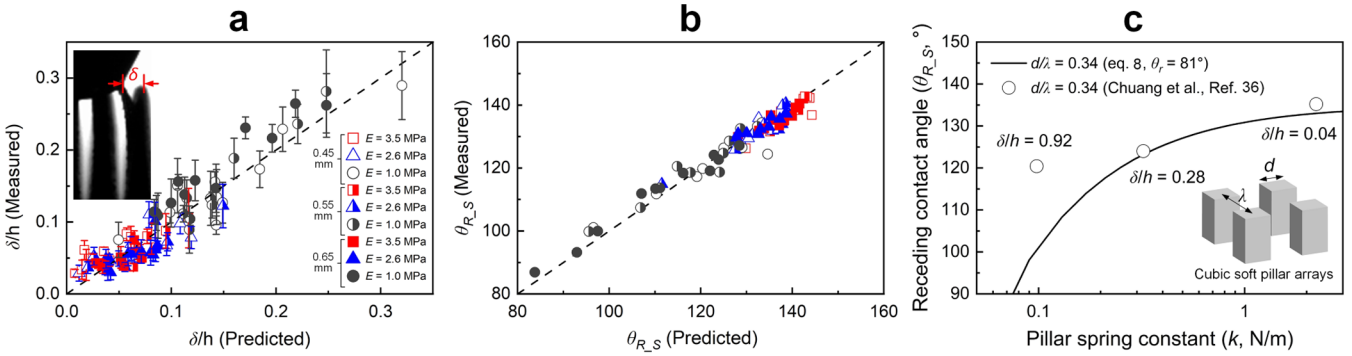

Figure 4. (a) Pillar deflection-to-height ratio (δ/h) measured from optical images is compared with the predicted ones using eq 6. (b) Measured droplet receding contact angles (θ_{R_S}) are plotted with the predicted ones using eq 8. The linear dashed lines with a slope of 1 serve as a guide for the eyes. (c) The droplet receding contact angles (θ_{R_S}) on soft pillar arrays measured by Chuang et al.[36] are compared with the predicted values using eq 8. Used with permission from ref 36. Copyright 2014, Royal Society of Chemistry.

$D - (D - d)z/h$. A small deflection of the beam is assumed for simplicity.[37] By solving the equation of $F(h - z) = EI(z)d^2x/dz^2$ with the boundary condition of $x(z = 0) = 0$ and $x'(z = 0) = 0$, the force−deflection relationship at the pillar top is expressed as

$$F = \frac{3\pi ED^3 d}{64h^3}\cdot\delta \tag{4}$$

where $3\pi ED^3d/64h^3$ can be identified as the spring constant k for linear elasticity. As shown in Figure 3, the horizontal point force F exerted on a single pillar, which results from the capillary force underneath the droplet and that at the outer droplet interface,[37] is given as

$$F = \gamma_{LV}\lambda(1 + \cos\theta_{\bar{R}}) \tag{5}$$

It should be noted that the angle $\theta_{\bar{R}}$ between the liquid−vapor interface and the horizontal plane is not a constant. Instead, as schematically shown in Figure 3b,c, it varies from around θ_r on the pillar top (it is a locally flat surface) to a value close to the droplet apparent receding contact angle in the middle of two pillars. Thus, it is not realistic to accurately estimate the angle, and for the sake of simplicity, $\theta_{\bar{R}}$ is taken as the average of θ_r and θ_{R_R} (θ_{R_R} is predicted by eq 2). Then, the top deflection δ of a conical pillar can be expressed as

$$\delta = \frac{F}{k} = \frac{64\gamma_{LV}\lambda(1 + \cos\theta_{\bar{R}})h^3}{3\pi ED^3 d} \tag{6}$$

By calculating the total strain energy equation of $\int_0^h (F^2(h - z)^2/2EI(z))\mathrm{d}z$, the energy stored in a deflected soft pillar (Δe_{DP}) is

$$\Delta e_{DP} = \frac{32h^3}{3\pi ED^3 d}\cdot F^2 = \frac{F^2}{2k} \tag{7}$$

Assuming the number of n pillars along the droplet perimeter deflect simultaneously, the total energy stored in pillars is $\Delta E_{DP} = nF^2/2k$. Inserting ΔE_{DP} into eq 3 and dividing $\gamma_{LV}n\lambda\Delta x$ on both sides, eq 3 gives the receding contact angle on soft pillar arrays (θ_{R_S}) as

$$\cos\theta_{R\_S} = \cos\theta_{R\_R} + \frac{\lambda}{d}\cdot\frac{\gamma_{LV}(1 + \cos\theta_{\bar{R}})^2}{2k} \tag{8}$$

The characteristic length scale of Δx is approximated as the pillar top diameter d because the contact line can only slide on pillar tops before it jumps to the next array of pillars.[14] Since the second term on the right-hand side of eq 8 must be positive, θ_{R_S} must be smaller than θ_{R_R}, agreeing with the first observation in Figure 2. Different from eq 2 that is applicable up to $d/\lambda = 1$ (a smooth surface), eq 8 is not applicable to $d/\lambda = 1$ because the second term on the right-hand side must vanish.

The $\cos\theta_{R\_R}$ (eq 2) in eq 8 may be subject to modifications if the pillar deflection affects the microscopic dynamics of the contact line and the liquid−vapor interface. Moreover, the substrate deformation (wetting ridge) caused by γ_{LV}, albeit negligibly small, may affect the nanoscopic contact angle, which means the intrinsic receding contact angle on the smooth surface θ_r is also subject to modifications for the estimation of $\cos\theta_{R\_R}$, especially for very soft materials. Here, for the sake of simplicity, this complicated coupling of pillar deflection and contact line dynamics and the quantification of the wetting ridge effect are out of the scope of this study and hence not considered.

To validate eq 8, we first examine the small deflection assumption by plotting the measured pillar top deflection-to-height ratios δ/h with the predicted ones using eq 6 in Figure 4a. The measured δ and δ/h are also listed in Table S1. The good agreement between the measured and predicted δ/h validates a small deflection assumption (linear elasticity). In Figure 4b, moreover, an excellent agreement between the measured apparent receding contact angles on soft pillar arrays (θ_{R_S}) with the predicted ones not only verifies eq 8 but also substantiates the role of pillar deflection in droplet depinning characteristics. The measured θ_{R_S} values are also listed in Table S1 together with their corresponding dimensions and mechanical properties.

To further corroborate eq 8, we compare the experimental θ_{R_S} on PDMS cubic pillar arrays reported by Chuang et al.,[36] which were prepared using conventional photolithography with pillar sizes in tens of microns. Table 1 summarizes their surface geometry and mechanical properties. Here, θ_r is taken as the one measured on the flat PDMS sample with a base-to-curing agent ratio of 10:1, that is, 81°. Figure 4c compares the measured θ_{R_S} (dots) and the predicted ones (line), where the spring constant k is $Ed^4/4h^3$ for cubic pillars. For the samples with k = 2.23 and 0.32 N/m, the measured θ_{R_S} are well captured by eq 8. However, θ_{R_S} is underpredicted on the sample with k = 0.10 N/m. We speculate that the violation of the small deflection assumption ($\delta/h = 0.92$ for the case of k =

https://doi.org/10.1021/acs.langmuir.3c02667
Langmuir 2023, 39, 15401−15408

Table 1. Geometric Dimensions, Mechanical Properties, and Measured Droplet Apparent Receding Contact Angles of the Soft Cubic Pillar Arrays Reported by Chuang et al.[36,a]

d/λ	d (μm)	λ (μm)	h (μm)	E (MPa)	k (N/m)	θ_{R_S} (deg)[b]	δ/h
0.34	9.9	29.1	16.1	3.87	2.23	135.2	0.04
0.34	9.9	29.1	16.1	0.56	0.32	124.0	0.28
0.34	9.9	29.1	16.1	0.17	0.10	120.4	0.92

[a]Used with permission from ref 36. Copyright 2014, Royal Society of Chemistry. [b]Only the θ_{R_S} measured by withdrawing the liquid from the droplet were adopted.

0.10 N/m) leads to the failure of prediction. By contrast, the two successful predictions correspond to δ/h of only 0.04 and 0.28.

Discussion of the Physical Implication of the Model. Upon the successful validation of eq 8, we examine the exclusive effects of k and d/λ on soft pillar arrays. Since θ_{R_R} and $\theta_{\bar{R}}$ [$\theta_{\bar{R}} = (\theta_r + \theta_{R\_R})/2$] are determined only by surface chemistry (θ_r) and pillar geometry (d/λ), θ_{R_S} should monotonously decrease with a decrease in k as given by eq 8 (k is in the denominator) when θ_r and d/λ are fixed. Therefore, the experimental data are categorized following d/λ, ranging from 0.08 to 0.53 (see Table S1 for details), to reveal the exclusive effects of the spring constant k. We choose data of $d/\lambda = 0.11$, $d/\lambda = 0.19$, and $d/\lambda = 0.25$ as examples and plot them with respect to k in Figure 5a. All measured θ_{R_S} (dots) decrease with the decrease in k, and this trend is well captured by the predicted ones (dashed lines) using eq 8. This confirms that a softer pillar (smaller k) results in a smaller θ_{R_S} as well as a larger deviation between θ_{R_S} and θ_{R_R}, agreeing with the second observation in Figure 2.

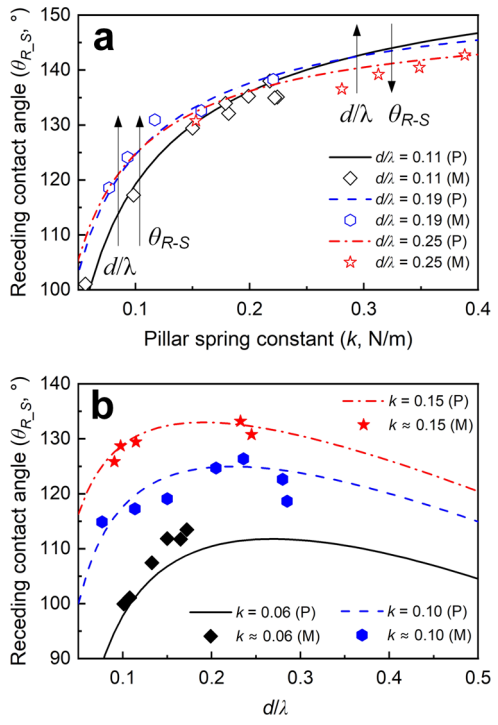

Figure 5. (a) For fixed values of the pillar packing density d/λ, measured (dots, M) and predicted (lines, P) θ_{R_S} are plotted with the pillar spring constant k. The symbols ↑↑ and ↑↓ represent regimes where θ_{R_S} increases and decreases with the increase in d/λ, respectively. (b) For fixed values of k (in a unit of N/m), measured (dots, M) and predicted (lines, P) θ_{R_S} are plotted with d/λ.

Most surprisingly, we observed the crossover of the lines (predicted at θ_{R_S}) for samples with different values of d/λ. Specifically, the predicted θ_{R_S} in Figure 5a demonstrates that for larger values of k (more rigid pillars), the surfaces with a smaller value of d/λ have larger receding contact angles. This agrees with the conventional understanding of rigid pillar arrays (eq 2), where the decrease in packing density results in easier droplet depinning and larger receding contact angles (see the dashed line in Figure 2).[9,10,14] By contrast, for smaller values of k (softer pillars), the surfaces with a smaller value of d/λ have smaller receding contact angles, which opposes eq 2.

This contrast between more rigid pillars (larger k) and softer pillars (smaller k) can be explained by the competitive effects of the first and second terms in eq 8, which are essentially controlled by the collective effects of pillar geometry (pillar packing density d/λ) and pillar mechanical properties (spring constant k). Given the fact that θ_{R_R} increases monotonously with the decrease in d/λ (see the dashed line in Figure 2), the first term on the right-hand side of eq 8 ($\cos\theta_{R\_R}$) is effectively proportional to d/λ. By contrast, the second term on the right-hand side $\gamma_{LV}\lambda(1 + \cos\theta_{\bar{R}})^2/2kd$ is inversely proportional to d/λ, indicating that a decrease in d/λ may lead to a decrease in θ_{R_S}. It should be noted that the decrease in d/λ leads to a decrease in $(1 + \cos\theta_{\bar{R}})^2$, but this effect is overshadowed by the λ/d. This contrasting dependency of the first and second terms of eq 8 on d/λ suggests that θ_{R_S} does not depend on d/λ monotonically.

To corroborate the above statements, we choose data with $k \approx 0.06$ N/m, 0.10 N/m, and 0.15 N/m as examples and plot them with respect to d/λ in Figure 5b. All data demonstrate an increase of θ_{R_S} with the increase in d/λ when d/λ are relatively small—a unique behavior to soft pillar arrays; when a certain value of d/λ and maxima of θ_{R_S} are reached, θ_{R_S} decreases with the increase in d/λ—well-known behavior for rigid pillar arrays. This explains the third observation in Figure 2 that eq 2 can still predict θ_{R_S} when $d/\lambda > 0.4$ because the soft pillar arrays behave similarly to rigid pillar arrays. Moreover, the critical d/λ at which the trend changes (the range of d/λ where θ_{R_S} increases with the increase in d/λ) increases with the decrease in k. It suggests that the unique trend of increasing θ_{R_S} with the increase in d/λ is more prominent for softer pillars (smaller k). This is because the second term of the right-hand side in eq 8 is also proportional to $1/k$ and therefore the value of k determines the relative weights (or contributions) of the first and the second terms. Nevertheless, the critical d/λ at which the dependency of θ_{R_S} on d/λ changes must be solved numerically and hence will not be included in this paper.

The counterintuitive droplet characteristics on the soft pillar arrays discussed above can be explained physically. Specifically, eq 8 is a modified form of eq 2 by considering the collective effects of capillarity and elasticity, where the capillary effect that deforms the pillar is reflected by $\gamma_{LV}(1 + \cos\theta_{\bar{R}})^2$, the elastic resistance against deformation is reflected by $2k$, and λ/d is a geometry factor. It is expected that λ works together with the capillary effect because a larger pillar spacing indicates more liquid−gas interfaces surrounding a pillar. On the other hand, the pillar diameter d works together with the elastic resistance. As such, the newly added term $\gamma_{LV}\lambda(1 + \cos\theta_{\bar{R}})^2/2kd$ is denoted as the *capillarity-to-elasticity ratio*, whose increase leads to an increasing deviation of the receding

https://doi.org/10.1021/acs.langmuir.3c02667
Langmuir 2023, 39, 15401−15408

contact angles on the soft pillar arrays from their counterparts on rigid pillar arrays ($\cos\theta_{R\_S} - \cos\theta_{R\_R}$).

As compared to rigid textured surfaces, the successful validation of eq 8 indicates that the surface adhesion property, e.g., the droplet receding contact angle, can be innovatively customized by varying the pillar height h and Young's modulus E (both affect k). Future studies are encouraged to investigate how pillar softness affects droplet adhesion by directly characterizing the droplet lateral and normal adhesion forces.[24,48,49] Moreover, this study only investigated pillars with axisymmetric shapes, e.g., conical pillars, where the spring constant k is isotropic and the pillar deflection is not direction-sensitive. Some surfaces exhibited directional adhesion, i.e., the droplet experiences different resistance forces at different motion directions, which is mainly attributed to the anisotropy in surface texture geometry and chemical coatings.[49] This study suggests that surface directional adhesion could be induced by the anisotropy in structure deflection, which may open a new route for droplet manipulation.

It should be noted that in addition to droplet receding contact angles studied here, droplet advancing and equilibrium contact angles are also important parameters in characterizing droplet characteristics. Nevertheless, we did not investigate the droplet advancing contact angle here mainly because the droplet advancing process (the wetting of the next array of pillars) is accomplished by the descending of the liquid−vapor interface onto pillar tops, and hence, the advancing contact angles are indifferent to pillar properties or geometries.[14,50,51] Regarding the equilibrium contact angle on the pillared substrate, it corresponds to the state with locally minimum energy and its derivation stems from the areal fraction of solid structures near the droplet boundary.[16,41,52,53] It is conceptually different from the receding contact angle that involves contact line sliding and liquid−vapor interface distortion, which is at the state with the locally highest energy. Thus, the equilibrium contact angle must be investigated in a separate study.

CONCLUSIONS

Prior investigations of droplet receding contact angles on superhydrophobic surfaces were mostly performed with rigid pillar arrays, where the pillar deflection or associated elastic energy was not considered. By systematically varying pillar geometric dimensions (pillar top diameter d, base diameter D, height h, and pitch λ) and its mechanical properties (Young's modulus E and the resulting spring constant k), we showed that models applicable to rigid pillar arrays failed to predict the apparent receding contact angles on soft pillar arrays. As such, we examined how pillar softness affects droplet receding contact angles, θ_{R_S}, and observed two interesting findings. First, in contrast to rigid pillar arrays, where a packing density d/λ typically corresponds to a specific receding contact angle, droplets exhibited a large range of receding contact angles on soft pillar arrays with a fixed d/λ but varying spring constant k. Second, the droplet receding contact angle could decrease with the decrease in d/λ on soft pillars, opposing the trend well-accepted for rigid pillars.[9,10,14] Those counterintuitive behaviors were attributed to the energy stored in the deflected soft pillars, which are controlled by collective effects of capillarity and elasticity. An analytical model was then developed to predict the droplet receding contact angles on soft pillar arrays with knowledge of the material intrinsic receding contact angle, pillar geometric dimensions, and pillar mechanical properties. This model was further verified by experiments conducted in this study and those reported by prior studies. The experimental results and theories reported in this study benefit various droplet-related applications such as wearable flexible electronics, soft robotics, biomedical devices, smart surfaces, etc.

ASSOCIATED CONTENT

Supporting Information

The Supporting Information is available free of charge at https://pubs.acs.org/doi/10.1021/acs.langmuir.3c02667.

Geometric dimensions and mechanical properties of the pillar arrays; measured droplet apparent receding contact angles on pillar arrays; and the measured pillar tip deflections of the soft pillars (PDF)

AUTHOR INFORMATION

Corresponding Author

Youhua Jiang − *Department of Mechanical Engineering (Robotics), Guangdong Technion—Israel Institute of Technology, Shantou, Guangdong 515063, China; Faculty of Mechanical Engineering, Technion—Israel Institute of Technology, Haifa 3200003, Israel; Guangdong Provincial Key Laboratory of Materials and Technologies for Energy Conversion, Guangdong Technion—Israel Institute of Technology, Shantou, Guangdong 515063, China;* orcid.org/0000-0002-6290-7789; Email: youhua.jiang@gtiit.edu.cn

Authors

Zhijia Xu − *Department of Mechanical Engineering (Robotics), Guangdong Technion—Israel Institute of Technology, Shantou, Guangdong 515063, China*

Bin Li − *Department of Mechanical Engineering (Robotics), Guangdong Technion—Israel Institute of Technology, Shantou, Guangdong 515063, China; Faculty of Mechanical Engineering, Technion—Israel Institute of Technology, Haifa 3200003, Israel; Guangdong Provincial Key Laboratory of Materials and Technologies for Energy Conversion, Guangdong Technion—Israel Institute of Technology, Shantou, Guangdong 515063, China;* orcid.org/0000-0002-1100-2058

Juan Li − *Department of Mechanical Engineering (Robotics), Guangdong Technion—Israel Institute of Technology, Shantou, Guangdong 515063, China; Faculty of Mechanical Engineering, Technion—Israel Institute of Technology, Haifa 3200003, Israel*

Dongshi Guan − *State Key Laboratory of Nonlinear Mechanics, Institute of Mechanics, Chinese Academy of Sciences, Beijing 100190, China; School of Engineering Science, University of Chinese Academy of Sciences, Beijing 100049, China;* orcid.org/0000-0002-4433-3662

Complete contact information is available at: https://pubs.acs.org/10.1021/acs.langmuir.3c02667

Author Contributions

Y.J.: conceptualization, investigation, supervision, methodology, formal analysis, writing—original draft, writing—review and editing, and funding acquisition. Z.X.: investigation. B.L.: writing—review and editing. J.L.: investigation. D.G.: writing—review and editing.

Notes

The authors declare no competing financial interest.

■ ACKNOWLEDGMENTS

This work was partially supported by the National Natural Science Foundation of China Nos. 12202108 and 11972351, the Guangdong Basic and Applied Basic Research Foundation Nos. 2021A1515110184, 2022A1515011214, and 2021B0301030005, and the Opening fund of State Key Laboratory of Nonlinear Mechanics.

■ REFERENCES

(1) Attinger, D.; Frankiewicz, C.; Betz, A. R.; Schutzius, T. M.; Ganguly, R.; Das, A.; Kim, C.-J.; Megaridis, C. M. Surface Engineering for Phase Change Heat Transfer: A Review. *MRS Energy Sustainability* **2014**, *1*, No. E4.
(2) Parent, O.; Ilinca, A. Anti-Icing and De-Icing Techniques for Wind Turbines: Critical Review. *Cold Reg. Sci. Technol.* **2011**, *65*, 88−96.
(3) Jiang, Y.; Machado, C.; Park, K.-C. K. From Capture to Transport: A Review of Engineered Surfaces for Fog Collection. *Droplet* **2023**, *2*, No. e55.
(4) Quéré, D. Wetting and Roughness. *Annu. Rev. Mater. Sci.* **2008**, *38*, 71−99.
(5) Jiang, Y.; Choi, C.-H. Droplet Retention on Superhydrophobic Surfaces: A Critical Review. *Adv. Mater. Interfaces* **2021**, *8*, No. 2001205.
(6) Butt, H.-J.; Liu, J.; Koynov, K.; Straub, B.; Hinduja, C.; Roismann, I.; Berger, R.; Li, X.; Vollmer, D.; Steffen, W.; Kappl, M. Contact Angle Hysteresis. *Curr. Opin. Colloid Interface Sci.* **2022**, *59*, No. 101574.
(7) Jiang, Y.; Sun, Y.; Drelich, J. W.; Choi, C.-H. Topography-Dependent Effective Contact Line in Droplet Depinning. *Phys. Rev. Lett.* **2020**, *125*, No. 184502.
(8) Lv, C.; Yang, C.; Hao, P.; He, F.; Zheng, Q. Sliding of Water Droplets on Microstructured Hydrophobic Surfaces. *Langmuir* **2010**, *26*, 8704−8708.
(9) Choi, W.; Tuteja, A.; Mabry, J. M.; Cohen, R. E.; McKinley, G. H. A Modified Cassie-Baxter Relationship to Explain Contact Angle Hysteresis and Anisotropy on Non-Wetting Textured Surfaces. *J. Colloid Interface Sci.* **2009**, *339*, 208−216.
(10) Raj, R.; Enright, R.; Zhu, Y.; Adera, S.; Wang, E. N. Unified Model for Contact Angle Hysteresis on Heterogeneous and Superhydrophobic Surfaces. *Langmuir* **2012**, *28*, 15777−15788.
(11) Li, D.; Xue, Y.; Lv, P.; Huang, S.; Lin, H.; Duan, H. Receding Dynamics of Contact Lines and Size-Dependent Adhesion on Microstructured Hydrophobic Surfaces. *Soft Matter* **2016**, *12*, 4257−4265.
(12) Qiao, S.; Li, S.; Li, Q.; Li, B.; Liu, K.; Feng, X.-Q. Friction of Droplets Sliding on Microstructured Superhydrophobic Surfaces. *Langmuir* **2017**, *33*, 13480−13489.
(13) Butt, H.-J.; Gao, N.; Papadopoulos, P.; Steffen, W.; Kappl, M.; Berger, R. Energy Dissipation of Moving Drops on Superhydrophobic and Superoleophobic Surfaces. *Langmuir* **2017**, *33*, 107−116.
(14) Jiang, Y.; Xu, W.; Sarshar, M. A.; Choi, C.-H. Generalized Models for Advancing and Receding Contact Angles of Fakir Droplets on Pillared and Pored Surfaces. *J. Colloid Interface Sci.* **2019**, *552*, 359−371.
(15) McHale, G. Cassie and Wenzel: Were They Really So Wrong? *Langmuir* **2007**, *23*, 8200−8205.
(16) Nosonovsky, M. On the Range of Applicability of the Wenzel and Cassie Equations. *Langmuir* **2007**, *23*, 9919−9920.
(17) Bormashenko, E. General Equation Describing Wetting of Rough Surfaces. *J. Colloid Interface Sci.* **2011**, *360*, 317−319.
(18) Reyssat, M.; Quéré, D. Contact Angle Hysteresis Generated by Strong Dilute Defects. *J. Phys. Chem. B* **2009**, *113*, 3906−3909.
(19) Sarshar, M. A.; Jiang, Y.; Xu, W.; Choi, C.-H. Depinning Force of a Receding Droplet on Pillared Superhydrophobic Surfaces: Analytical Models. *J. Colloid Interface Sci.* **2019**, *543*, 122−129.
(20) Fan, J.; De Coninck, J.; Wu, H.; Wang, F. Microscopic Origin of Capillary Force Balance at Contact Line. *Phys. Rev. Lett.* **2020**, *124*, No. 125502.
(21) Guan, D.; Wang, Y. J.; Charlaix, E.; Tong, P. Asymmetric and Speed-Dependent Capillary Force Hysteresis and Relaxation of a Suddenly Stopped Moving Contact Line. *Phys. Rev. Lett.* **2016**, *116*, No. 066102.
(22) Huang, X.; Fan, J.; Wu, H.; Wang, F. Local Molecular Asymmetry Mediated Self-Adaptive Pinning Force on the Contact Line. *Colloids Surf., A* **2023**, *674*, No. 131987.
(23) Tadmor, R. Approaches in Wetting Phenomena. *Soft Matter* **2011**, *7*, 1577−1580.
(24) Tadmor, R. Open Problems in Wetting Phenomena: Pinning Retention Forces. *Langmuir* **2021**, *37*, 6357−6372.
(25) Cassie, A. B. D.; Baxter, S. Wettability of Porous Surfaces. *Trans. Faraday Soc.* **1944**, *40*, 546−551.
(26) Shin, H.; Jo, S.; Mikos, A. G. Biomimetic Materials for Tissue Engineering. *Biomaterials* **2003**, *24*, 4353−4364.
(27) Shepherd, R. F.; Ilievski, F.; Choi, W.; Morin, S. A.; Stokes, A. A.; Mazzeo, A. D.; Chen, X.; Wang, M.; Whitesides, G. M. Multigait Soft Robot. *Proc. Natl. Acad. Sci. U.S.A.* **2011**, *108*, 20400−20403.
(28) Keplinger, C.; Sun, J.-Y.; Foo, C. C.; Rothemund, P.; Whitesides, G. M.; Suo, Z. Stretchable, Transparent, Ionic Conductors. *Science* **2013**, *341*, 984−987.
(29) Wei, C.; Zong, Y.; Jiang, Y. Bioinspired Wire-on-Pillar Magneto-Responsive Superhydrophobic Arrays. *ACS Appl. Mater. Interfaces* **2023**, *15*, 24989−24998.
(30) Style, R. W.; Jagota, A.; Hui, C.-Y.; Dufresne, E. R. Elastocapillarity: Surface Tension and the Mechanics of Soft Solids. *Annu. Rev. Condens. Matter Phys.* **2017**, *8*, 99−118.
(31) Bico, J.; Reyssat, É.; Roman, B. Elastocapillarity: When Surface Tension Deforms Elastic Solids. *Annu. Rev. Fluid Mech.* **2018**, *50*, 629−659.
(32) Chen, L.; Bonaccurso, E.; Gambaryan-Roisman, T.; Starov, V.; Koursari, N.; Zhao, Y. Static and Dynamic Wetting of Soft Substrates. *Curr. Opin. Colloid Interface Sci.* **2018**, *36*, 46−57.
(33) Andreotti, B.; Snoeijer, J. H. Statics and Dynamics of Soft Wetting. *Annu. Rev. Fluid Mech.* **2020**, *52*, 285−308.
(34) Guan, D.; Charlaix, E.; Tong, P. State and Rate Dependent Contact Line Dynamics over an Aging Soft Surface. *Phys. Rev. Lett.* **2020**, *124*, No. 188003.
(35) Chen, L.; Bonaccurso, E.; Shanahan, M. E. R. Inertial to Viscoelastic Transition in Early Drop Spreading on Soft Surfaces. *Langmuir* **2013**, *29*, 1893−1898.
(36) Chuang, Y.-C.; Chu, C.-K.; Lin, S.-Y.; Chen, L.-J. Evaporation of Water Droplets on Soft Patterned Surfaces. *Soft Matter* **2014**, *10*, 3394−3403.
(37) Papadopoulos, P.; Pinchasik, B.-E.; Tress, M.; Vollmer, D.; Kappl, M.; Butt, H.-J. Wetting of Soft Superhydrophobic Micropillar Arrays. *Soft Matter* **2018**, *14*, 7429−7434.
(38) Dev, A. A.; Dey, R.; Mugele, F. Behaviour of Flexible Superhydrophobic Striped Surfaces During (Electro-)Wetting of a Sessile Drop. *Soft Matter* **2019**, *15*, 9840−9848.
(39) Garcia-Gonzalez, D.; Snoeijer, J.; Kappl, M.; Butt, H.-J. Onset of Elasto-Capillary Bundling of Micropillar Arrays: A Direct Visualization. *Langmuir* **2020**, *36*, 11581−11588.
(40) Coux, M.; Kolinski, J. M. Surface Textures Suppress Viscoelastic Braking on Soft Substrates. *Proc. Natl. Acad. Sci. U.S.A.* **2020**, *117*, 32285−32292.
(41) Liu, B.; Tang, J.; Li, J.; Shan, Y.; Jiang, Y. Soft Wetting: Modified Cassie-Baxter Equation for Soft Superhydrophobic Surfaces. *Colloids Surf., A* **2023**, *677*, No. 132348.
(42) Jiang, Y. Droplet Depinning on Superhydrophobic Surfaces: From Simple Rigid Wetting to Complex Soft Wetting. *Surf. Innov.* **2022**, *10*, 373−378.

https://doi.org/10.1021/acs.langmuir.3c02667
Langmuir 2023, 39, 15401−15408

(43) Yuan, Q.; Zhao, Y.-P. Wetting on Flexible Hydrophilic Pillar-Arrays. *Sci. Rep.* **2013**, *3*, No. 1944.
(44) Roman, B.; Bico, J. Elasto-Capillarity: Deforming an Elastic Structure with a Liquid Droplet. *J. Condens. Matter Phys.* **2010**, *22*, No. 493101.
(45) Chandra, D.; Yang, S. Stability of High-Aspect-Ratio Micropillar Arrays against Adhesive and Capillary Forces. *Acc. Chem. Res.* **2010**, *43*, 1080−1091.
(46) Butt, H.-J.; Semprebon, C.; Papadopoulos, P.; Vollmer, D.; Brinkmann, M.; Ciccotti, M. Design Principles for Superamphiphobic Surfaces. *Soft Matter* **2013**, *9*, 418−428.
(47) Leh, A.; N'guessan, H. E.; Fan, J.; Bahadur, P.; Tadmor, R.; Zhao, Y. On the Role of the Three-Phase Contact Line in Surface Deformation. *Langmuir* **2012**, *28*, 5795−5801.
(48) Drelich, J. W.; Boinovich, L.; Chibowski, E.; Della Volpe, C.; Hołysz, L.; Marmur, A.; Siboni, S. Contact Angles: History of over 200 Years of Open Questions. *Surf. Innov.* **2020**, *8*, 3−27, DOI: 10.1680/jsuin.19.00007.
(49) Feldmann, D.; Pinchasik, B.-E. How Droplets Move on Surfaces with Directional Chemical Heterogeneities. *J. Phys. Chem. Lett.* **2021**, *12*, 11703−11709.
(50) Schellenberger, F.; Encinas, N.; Vollmer, D.; Butt, H. J. How Water Advances on Superhydrophobic Surfaces. *Phys. Rev. Lett.* **2016**, *116*, No. 096101.
(51) Jiang, Y.; Sun, Y.; Drelich, J. W.; Choi, C.-H. Spontaneous Spreading of a Droplet: The Role of Solid Continuity and Advancing Contact Angle. *Langmuir* **2018**, *34*, 4945−4951.
(52) Marmur, A. Solid-Surface Characterization by Wetting. *Annu. Rev. Mater. Res.* **2009**, *39*, 473−489.
(53) Ruiz-Cabello, F. J. M.; Rodríguez-Valverde, M. A.; Cabrerizo-Vílchez, M. A. Equilibrium Contact Angle or the Most-Stable Contact Angle? *Adv. Colloid Interface Sci.* **2014**, *206*, 320−327.

https://doi.org/10.1021/acs.langmuir.3c02667
Langmuir 2023, 39, 15401−15408